RESEARCH ARTICLE | DECEMBER 26 2023

Comparison of quantum well structures for room temperature continuous wave 980 nm lasers grown on (001) Si by MOCVD FREE

Jie Huang ; Qi Lin ; Wei Luo ; Wen Gu ; Liying Lin ; Kei May Lau

Appl. Phys. Lett. 123, 261101 (2023)
https://doi.org/10.1063/5.0179895

Applied Physics Letters ARTICLE pubs.aip.org/aip/apl

Comparison of quantum well structures for room temperature continuous wave 980 nm lasers grown on (001) Si by MOCVD

Cite as: Appl. Phys. Lett. **123**, 261101 (2023); doi: 10.1063/5.0179895
Submitted: 5 October 2023 · Accepted: 9 December 2023 ·
Published Online: 26 December 2023

Jie Huang,[1] Qi Lin,[1] Wei Luo,[1] Wen Gu,[1] Liying Lin,[1] and Kei May Lau[1,2,a)]

AFFILIATIONS

[1]Department of Electronic and Computer Engineering, Hong Kong University of Science and Technology, Clear Water Bay, Kowloon, Hong Kong, China
[2]Division of Emerging Interdisciplinary Areas, Hong Kong University of Science and Technology, Clear Water Bay, Kowloon, Hong Kong, China

[a)]Author to whom correspondence should be addressed: eekmlau@ust.hk

ABSTRACT

We report room temperature (RT) continuous-wave (CW) lasing of quantum well (QW) lasers grown on (001) Si substrates emitting at 980 nm. Two different QW structures, including conventional compressively strained InGaAs/GaAs QWs and strain-compensated InGaAs/GaAs/GaAsP QWs, were investigated. Photoluminescence properties and device performance of both structures on native GaAs and (001) Si substrates are discussed. By adding GaAsP barriers to the InGaAs/GaAs QWs, the lowest threshold current density of ridge waveguide edge-emitting QW lasers obtained on Si is 550 A/cm^2, measured on a 10 μm × 2 mm device at RT. The working temperature of the InGaAs/GaAs/GaAsP QW lasers grown on Si can be over 95 °C in the CW mode. This work suggests a feasible approach to improve the 980 nm laser performance on Si for monolithic optoelectronic integration.

Silicon is the most widely used material in conventional electronic circuits for data processing. For nearly three decades, Si-based photonic integrated circuits (PICs) made compatible with CMOS technologies have been investigated and adopted, offering major benefits in large bandwidth and low power consumption.[1–3] On-chip efficient III–V light sources are essential building blocks for PICs because of their superior optical properties and demonstrated performance.[4,5] Although high-performance lasers grown on native III–V wafers have been transferred onto Si substrate by die or wafer bonding techniques, monolithic epitaxial growth of III–V lasers on Si offers an attractive alternative to eliminate difficulties in high-precision alignment steps.[6–8] Since many dissimilarities exist between III–V materials and Si, significant challenges in heteroepitaxial growth such as antiphase boundaries (APBs), large thermal expansion coefficient mismatch, and high threading dislocation densities (TDDs) are yet to be fully resolved.[9–11] To address these issues, various techniques have been investigated. APBs can be eliminated by utilizing optimized Si wafer pretreatment,[12] patterned Si[13] and Si wafers with offcut toward ⟨001⟩.[14] Meanwhile, growth approaches including strained-layer dislocation filters (DFs),[15,16] compositionally graded buffers,[17,18] and thermal cycle annealing (TCA)[19,20] have been explored to reduce crystalline defects resulting from heteroepitaxy. The problem of surface cracks caused by large thermal expansion coefficient mismatch could be alleviated with lower cooling down speed after growth.[21] Heteroepitaxial growth of efficient coherent light sources on Si has been motivated by the demand for large capacity in data centers that need high performance and reliable III–V lasers in the communication bands.[2] Quantum well (QW) lasers emitting at different bands have been demonstrated on Si in recent years.[17,22] In addition, lasers emitting at 980 nm can be used as a pumping source for erbium-doped fiber amplifiers for optical fiber communication systems since it offers advantages of larger gain coefficient and multi/demultiplex operation for pumping.[23] Recently, the 980 nm InGaAs/AlGaAs quantum well (QW) lasers grown on Si have been demonstrated, but the lifetime of the laser is only 90 s, and the operation at high temperatures (above 25 °C) is not shown.[24]

Here, we compare the performance of 980 nm QW lasers with two distinct QW structures grown on both native GaAs and Si substrates to investigate the impact of GaAsP barrier layers on device performance. The growth and performance of the two different QW

structures were investigated, including their photoluminescence (PL) characteristics and device performance at different temperatures. Preliminary results have revealed that the strain-compensated InGaAs/GaAs/GaAsP QW lasers exhibited lower threshold current densities and better temperature stability than conventional InGaAs/GaAs QW laser structures grown on both GaAs and (001) Si substrates.

The growth of GaAs-on-planar Si (GoPS) templates and laser structures were performed at 100 mbar in an AIXTRON close coupled showerhead (CCS) and an AIXTRON 200/4 metal organic chemical vapor deposition (MOCVD) system, respectively. Commercial nominal (001) Si wafer (~0.5° offcut with random orientation) was first cleaned in boiling $NH_4OH:H_2O_2:H_2O$ (1:1:5) solution for 10 min and was dipped in 1% HF solution for 90 s to remove the native oxide. The as-treated Si wafer was then transferred into the reactor for subsequent growth. After annealing at 850 °C for 15 min in a pure H_2 ambient to assist the formation of bi-atomic terraces, a uniform GaAs nucleation layer (~10 nm) was deposited first at 400 °C. Then two layers of GaAs with a total thickness of 950 nm were grown at 510 and 560 °C, respectively. Subsequently, four cycles of TCA were applied with temperature cycling between 330 °C (5 min) and 680 °C (5 min), after which a 150 nm GaAs layer was grown at 560 °C. To further improve the quality of the GaAs film on (001) Si, the GoPS templates were heated to 730 °C in an arsenic ambient for 4 min and then cooled down to 330 °C (5 min) for six cycles after completing the growth of a 350 nm GaAs layer. Ten periods of 9.5 nm $In_{0.15}Ga_{0.85}As$/12 nm GaAs strained-layer superlattices (SLSs) were grown to further filter the threading dislocations (TDs). Finally, a 300 nm GaAs layer was grown on top, as illustrated in Fig. 1(a). Figure 1(b) shows a $10 \times 10\ \mu m^2$ atomic force microscope (AFM) image of the 2 μm-thick GoPS templates, with a root mean square (RMS) value of 1.43 nm. The cross-sectional transmission electron microscopy (X-TEM) image of the GoPS templates is displayed in Fig. 1(c). A high density of crystalline defects generated at the GaAs/Si hetero-interface propagates toward the interface between the SLSs and GaAs. The propagation of TDs was bent by the strain fields of the SLSs, and their glide direction was changed into the (001) plane. Additionally, the interaction between TDs during TCA also contributes to the reduction in TDDs. Figure 1(d) depicts a representative plane-view TEM (PV-TEM) image of the 2 μm-thick GoPS templates. A total scanned area of ~200 μm^2 was observed to obtain a defect density value of $2.8 \times 10^7\ cm^{-2}$.

Two types of QW structures were designed to investigate the effect of tensile-strained GaAsP barriers on the performance of QWs, as schematically delineated in Figs. 2(a) and 2(b). Prior to the growth of QWs, a uniform GaAs layer (100 nm) was first grown on a GaAs substrate and a 2 μm-thick GoPS template simultaneously in the same run. For the QW1 structure, two 5 nm $In_{0.18}Ga_{0.82}As$ QWs were sandwiched by GaAs barriers, which were then capped with 40 nm $Al_{0.2}Ga_{0.8}As$ and 40 nm $Al_{0.4}Ga_{0.8}As$ cladding layers. Two strain-compensated $In_{0.18}Ga_{0.82}As$/GaAs/$GaAs_{0.87}P_{0.13}$ QW structures were stacked in the QW2 structure. Two 6 nm GaAs layers acted as barriers of the $In_{0.18}Ga_{0.82}As$ QWs, surrounded by two $GaAs_{0.87}P_{0.13}$ layers. The compositions of indium and phosphorus in the QW structures were measured by energy dispersive spectroscopy. Figure 2(c) illustrates the band diagram of the QW1 and QW2 structures. Compared to QW1, the thermal escape probability of electrons in QW2 could be reduced by introducing GaAsP barriers. Figure 2(d) plots the PL spectra of the as-grown QW structures grown on the GaAs substrates excited by a 514 nm continuous-wave (CW) diode laser at room temperature (RT, 20 °C). The PL peak of QW2 is stronger (6%) and narrower, with a full width at half maximum (FWHM) of 26 meV, compared to that of QW1 (34 meV). The shoulders (912 and 915 nm) in the PL spectra of QW1 and QW2 are presumably the ground state electron-light hole band (1e–1lh) recombination in the InGaAs QWs due to the splits of the valence band.[25] The PL spectra of QW1 and QW2 grown on the 2 μm-thick GoPS templates are plotted in the inset of Fig. 2(d). The PL intensity of QW2 is 22% stronger than that of QW1, and the PL linewidth of QW2 is 5% narrower than that of

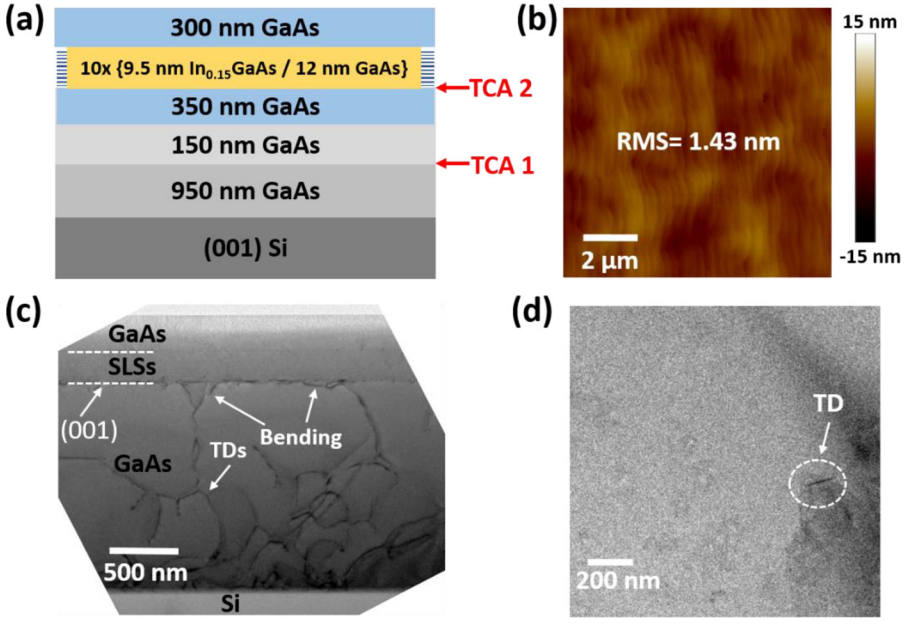

FIG. 1. (a) Schematic diagram of 2 μm-thick GoPS templates with two sets of TCA and ten periods of SLSs. (b) $10 \times 10\ \mu m^2$ AFM image of GoPS templates with an RMS value of 1.43 nm. The color scale of the AFM image is 30 nm. (c) X-TEM and (d) PV-TEM images of a 2 μm-thick GoPS template. Interaction and bending of TDs took place obviously in the GaAs epilayer.

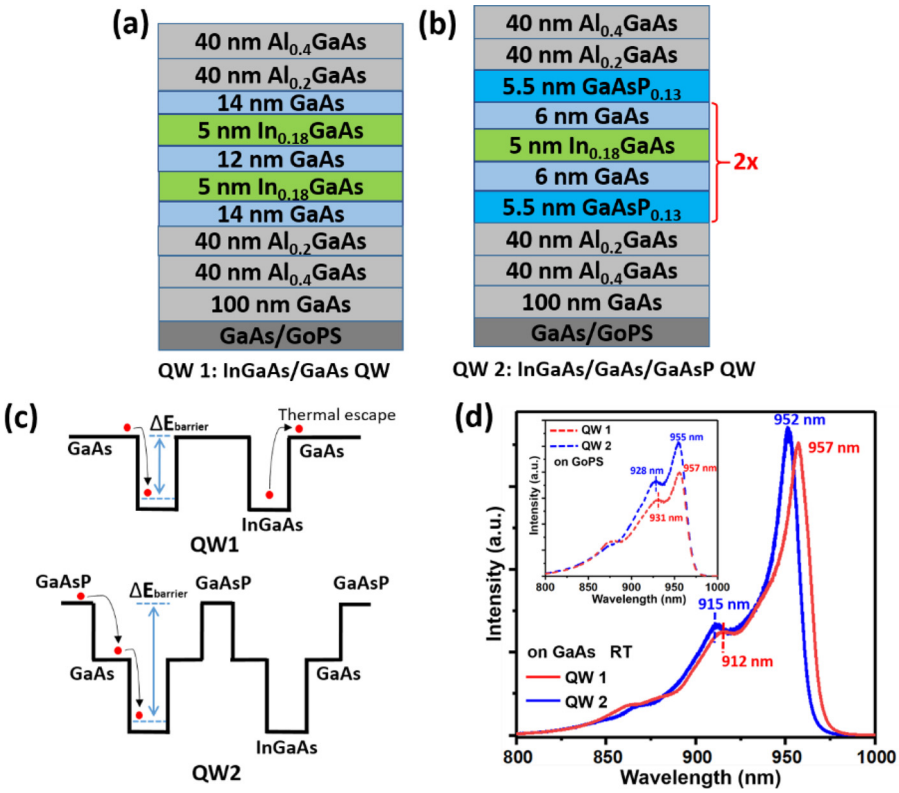

FIG. 2. Schematic diagrams of (a) $In_{0.18}Ga_{0.82}As/GaAs$ QWs (QW1) and (b) $In_{0.18}Ga_{0.82}As/GaAs/GaAs_{0.87}P_{0.13}$ QWs (QW2) grown on GaAs and the GoPS templates. (c) Schematic diagram of QW1 and QW2. (d) PL spectra of QW1 and QW2 grown on GaAs. Inset is the PL spectra of two QW structures grown on GoPS templates.

QW1. The insertion of the tensile-strained GaAsP barriers contributes to the PL linewidth narrowing of QW2 on both GaAs substrates and GoPS templates. Since the PL linewidth is related to the interface between the barriers and QWs in the QW structure, fluctuations in well width would lead to broadening of the band edges.[26] The QW2 structure shows smoother interfaces than QW1, as evidenced by the zoomed-in cross sectional TEM images in Figs. 3(c) and 3(d). The relative difference between the PL intensities of the peaks in QW1 and QW2 grown on GoPS templates (22%) is larger than these two QW structures on GaAs substrates (6%), which could be ascribed to the residue strain in the GoPS templates, resulting from the 4% lattice mismatch between the GaAs buffer and Si, as well as the growth of InGaAs/GaAs SLSs.[19] The differential gain tends to saturate as the amount of the compressive strain increases.[27] The accumulation of compressive strain could be alleviated by the insertion of tensile-strained GaAsP layers. Furthermore, tensile-strained GaAsP barriers not only increases the band offset and splitting between the highest heavy-hole and light hole states but also promote the energy increase in the sub-bands of the wells, thereby causing a slight blue shift of the PL peak wavelength in QW2 on both GaAs substrates and GoPS templates.[28]

After the gain region optimization, laser structures with different active regions were grown on both GaAs substrates and the GoPS templates. The growth sequence was as follows: 700 nm *n*-type GaAs contact layer, 800 nm *n*-type $Al_{0.7}GaAs$ cladding, active region, 800 nm *p*-type $Al_{0.7}GaAs$ cladding, and 200 nm *p*-type GaAs contact layer. The doping concentrations of the *n*-type GaAs contact and the $Al_{0.7}GaAs$ cladding layer were 1×10^{19} and $6.9 \times 10^{17}\,cm^{-3}$, respectively. The doping concentrations of the *p*-type $Al_{0.7}GaAs$ cladding and the GaAs contact layer were 1.6×10^{18} and $4.6 \times 10^{19}\,cm^{-3}$, respectively. A schematic diagram of the whole laser structure with QW2 is depicted in Fig. 3(a). The global-view of a cross-sectional scanning transmission electron microscopy (STEM) image of the QW2 laser structure grown on the GoPS templates is shown in Fig. 3(b), with the zoomed-in STEM image of the active region displayed in Fig. 3(c). From the STEM image, the thickness of each layer in the active region is the same as designed, and the InGaAs/GaAs/GaAsP QWs feature sharp interfaces on the GoPS templates. Figure 3(d) shows the zoomed-in STEM image of the InGaAs/GaAs QWs in the QW1 laser structure, and the interfaces in compressively strained InGaAs/GaAs QW are not as sharp as that in the strain-compensated InGaAs/GaAs/GaAsP QWs.

To investigate the device performance of the lasers with QW1 and QW2 active regions, ridge waveguide edge-emitting lasers were fabricated. The fabrication process with detailed steps have been described in our previous publications.[29,30] The cleaved laser bars on different substrates were placed on a heated stage with a temperature controller and electrically driven by continuous current at various temperatures. Figure 4(a) presents representative current–voltage (I–V) curves of QW1 and QW2 lasers with the same size (10 μm ridge width and 2 mm cavity length) grown on GoPS templates. The I–V characteristics of these two devices are comparable. The turn-on voltage of lasers is measured to be ~1.1 V and the series resistance ranges 10–14 Ω. Figure 4(b) shows a representative RT emission spectra of a 10 μm × 1.2 mm QW2 laser grown on the GoPS templates under the CW condition. The lasing spectra was measured by coupling the

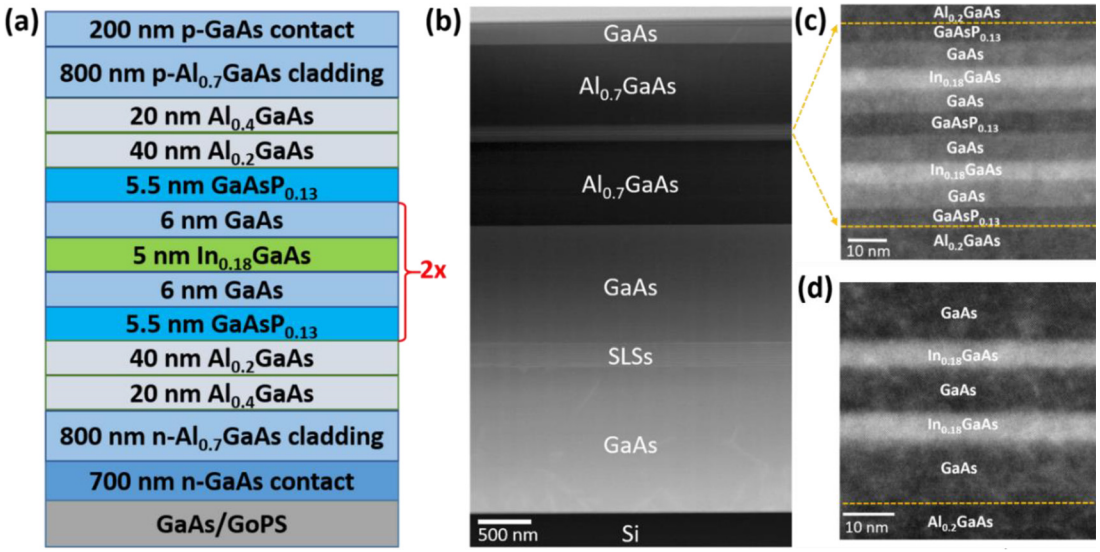

FIG. 3. (a) Schematic of electrically pumped QW2 laser grown on GaAs substrate and GoPS templates. (b) Global-view cross-sectional STEM image of QW2 laser grown on GoPS templates. (c) Zoomed-in STEM image of the active region. (d) STEM image of InGaAs/GaAs QWs in the QW1 laser structure grown on GoPS templates.

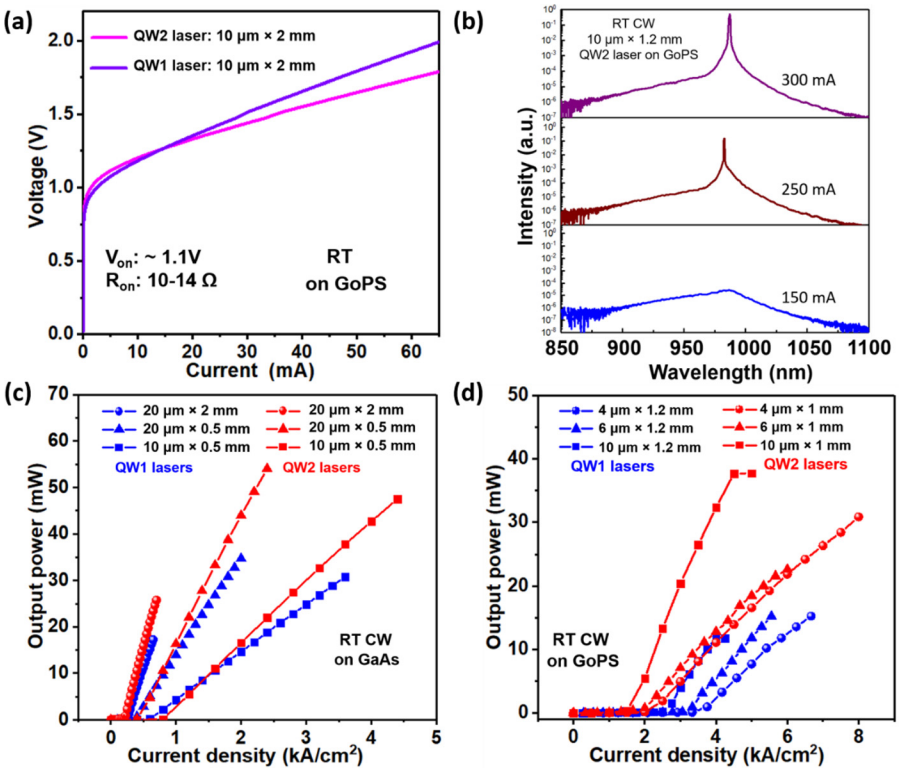

FIG. 4. (a) I–V curves of QW1 and QW2 lasers grown on GoPS templates. (b) RT emission spectra of a 10 μm × 1.2 mm QW2 laser grown on GoPS templates at various injection current. Light vs current density curves of lasers with different QW structures on (c) GaAs and (d) GoPS templates.

output light into a lensed fiber connected to an optical spectrum analyzer. The transition from spontaneous emission to primary lasing at 983 nm is evident from the sudden narrowing of the emission envelope when the injection current is above the threshold.

Representative light vs current-density characteristics of the lasers grown on GaAs substrates with different dimensions are shown in Fig. 4(c). Compared with QW2 lasers, QW1 lasers of the same size show comparable threshold but a smaller slope efficiency. The

threshold is mainly related to gain of QWs and loss within the cavity. The slope efficiency is influenced by the internal quantum efficiency (IQE) and absorption loss, particularly free carrier absorption losses. The QW2 structure has a higher IQE compared to QW1, thereby accounting for the difference in their respective slope efficiency. Moreover, the larger slope efficiency of QW2 lasers could also be ascribed to the elevated band offset of the conduction and valence band after insertion of GaAsP barriers.[31–33] Figure 4(d) displays light vs current-density curves of QW1 and QW2 lasers grown on the GoPS templates. The threshold current densities of QW2 lasers are obviously lower than that of QW1 lasers when devices have similar dimensions, which is consistent with the PL spectra shown in Fig. 2(d). The total strain in the active region accumulates with the growth of the compressively strained InGaAs layer on GoPS, and lattice misfit dislocations would start to form in the active region when the total strain approaches the critical level.[28] In addition to better carrier confinement, the accumulated compressive strain of the InGaAs layer in the active region can be compensated by the GaAsP barrier, resulting in somewhat better crystalline quality of QW2.

To benchmark the thresholds of QW lasers on GaAs substrates and GoPS templates at RT under CW condition, statistical data of QW1 and QW2 lasers with different sizes (width: 2–40 μm, length: 0.5–2 mm) are summarized in Fig. 5(a). The average lasing threshold current density of the QW1 lasers on GaAs substrates is comparable to that of QW2 lasers. The QW1 lasers grown on GoPS templates with an average threshold current density of 3.83 kA/cm^2 show a more dispersed distribution, while the lasing thresholds of QW2 lasers are more clustered and spread from 0.55 to 3.33 kA/cm^2. More than 50 devices have been measured for each QW laser structure on GoPS templates for fair comparison. Figures 5(b) and 5(c) plot the threshold current density vs cavity length for both QW1 and QW2 lasers grown on GoPS templates with a fixed ridge width of 4 and 6 μm, respectively. Compared to QW2 lasers, QW1 laser with same dimensions on Si shows a larger threshold. We ascribe the large difference in the average threshold between the QW1 and QW2 lasers on Si to the larger band offset and strain compensation of the InGaAs/GaAs/GaAsP QWs we adopted.

To evaluate the temperature characteristics of these two different QW laser structures and minimize thermal effects caused by CW injection current, measurements of light–current (L–I) curves and spectra were performed on GaAs substrates and GoPS templates under pulsed mode in the temperature range from 25 to 95 °C. Figure 6(a) plots the temperature dependence of threshold currents of the two QW laser structures on GaAs substrates, with extracted characteristic temperatures T_0. The T_0 of QW1 laser was fitted to be 137 K, which is lower than that of the QW2 laser (154.5 K). Figure 6(b) displays the temperature dependence of the lasing peak ($d\lambda/dT$) at a fixed injection current, showing essentially no difference between the two. The T_0 of QW1 laser on GoPS templates was extracted to be 66 K in the temperature range of 25–85 °C, as shown in Fig. 6(c). A T_0 value of 97 K and a $d\lambda/dT$ of 0.35 nm/°C were obtained on the QW2 laser. The QW1 and QW2 lasers have the same trend of T_0 and $d\lambda/dT$ on GaAs and GoPS templates. The lower T_0 and larger $d\lambda/dT$ on QW1 lasers shows that QW2 lasers have better high-temperature stability on both GaAs substrate and GoPS templates. It can be ascribed to the reduced thermal escape probability of electrons from the active region at high temperature by introducing GaAsP barriers.[34]

The temperature dependence of threshold currents of the QW1 and QW2 lasers with similar dimensions on GaAs substrates operating in CW mode are shown in Fig. 7(a). The characteristic temperature T_0 of a QW2 laser grown on GaAs substrates was extracted to be ~140 K, while the T_0 of a QW1 laser was 129.6 K below 60 °C and decreased to 103.4 K from 60 to 95 °C, indicating inferior temperature stability of InGaAs/GaAs QWs at high temperatures. Measured L–I curves of QW1 and QW2 lasers on GoPS templates at progressively increasing temperatures are plotted in Figs. 7(b)–7(d). The T_0 of QW1 laser was extracted to be ~34.5 K from 25 to 45 °C as exhibited in the inset of Fig. 7(b). Meanwhile, the QW1 laser could lase at a temperature not higher than 45 °C and degraded rapidly. Compared with the QW1 laser, the QW2 lasers on GoPS templates could lase up to 90 °C and even higher than 95 °C under CW operation (limited by the setup), and no significant slope efficiency drop was observed with the increase in temperature. A high T_0 of a 4 μm × 1 mm QW2 laser was extracted to be 103 K from 25 to 70 °C and decreased to 36.6 K from 70 to 90 °C [inset of Fig. 7(c)]. The 2 μm × 1.5 mm QW2 laser can lase above 95 °C, as shown in Fig. 7(d). In QW1 lasers, carriers escaping from the active region at higher temperatures give rise to degradation of the laser performance, thus leading to the reduction in gain and higher non-radiative recombination. The carrier escape could be alleviated by the insertion of GaAsP barriers with better carrier confinement.[35]

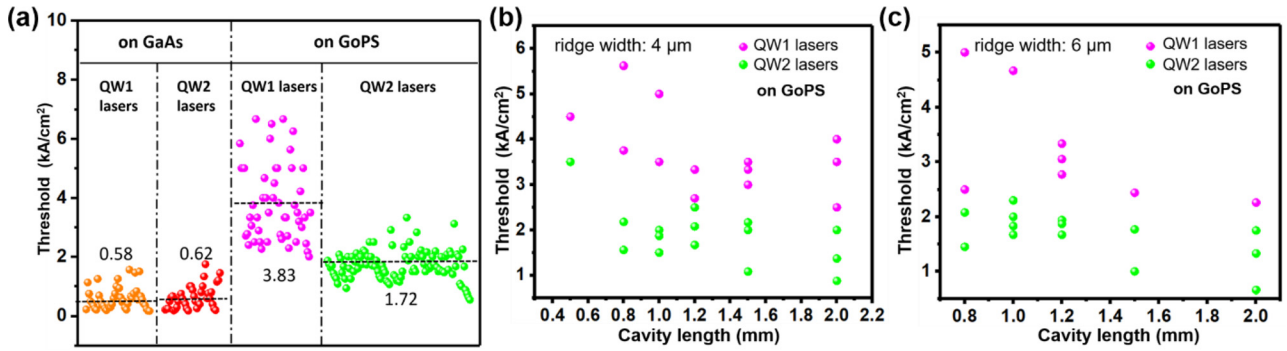

FIG. 5. (a) Threshold current densities of QW1 and QW2 lasers with different sizes on GaAs substrates and the GoPS templates. Plot of threshold current density vs cavity length for both QW1 and QW2 lasers on GoPS with a fixed ridge width of (b) 4 μm and (c) 6 μm.

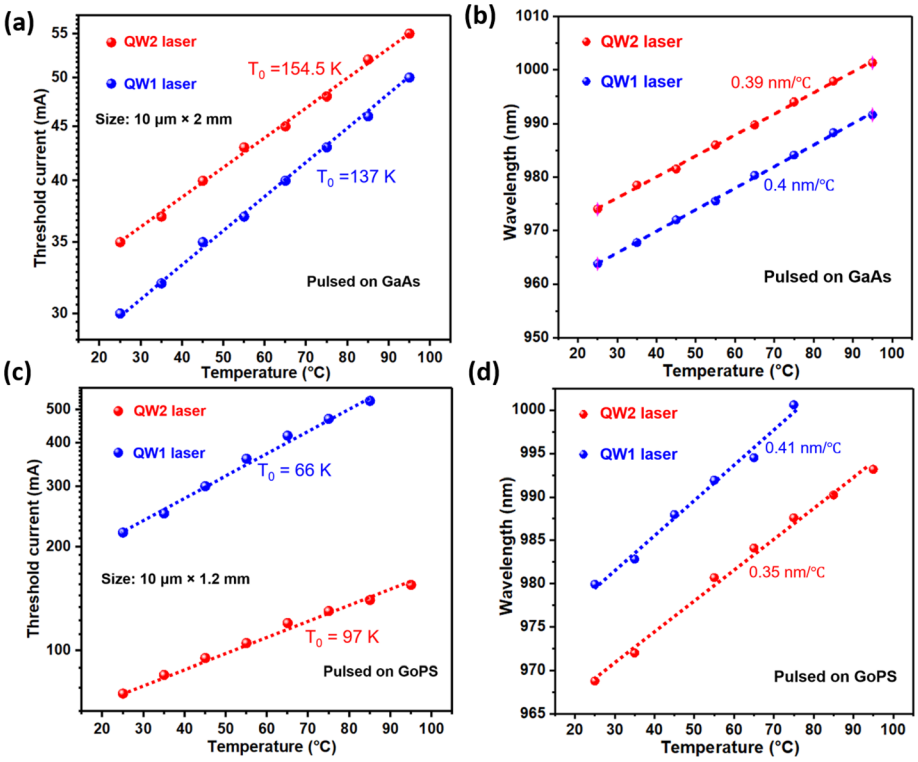

FIG. 6. (a) Lasing threshold currents of QW1 and QW2 lasers on GaAs at different temperatures under the pulse mode and (b) the corresponding lasing peak-shift. (c) Lasing threshold currents of QW1 and QW2 lasers on GoPS at different temperatures under the pulse mode and (d) the corresponding lasing peak-shift.

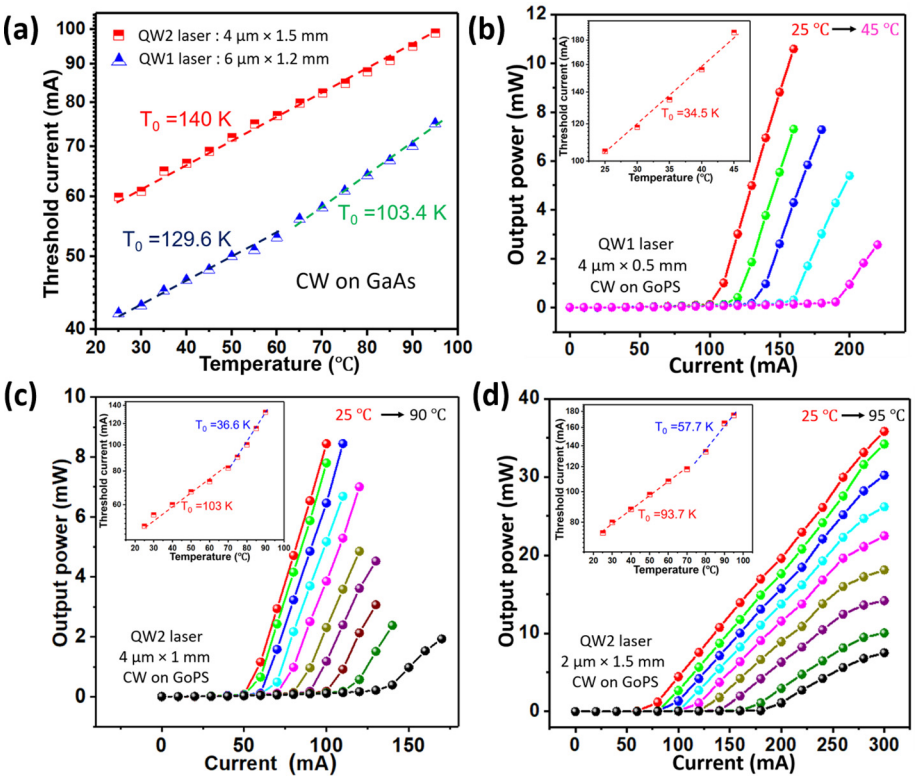

FIG. 7. (a) CW lasing threshold currents of QWs lasers on GaAs at different temperatures. (b) Measured L–I curves from a 4 μm × 0.5 mm QW1 laser on GoPS as a function of temperature under the CW mode with the characteristic temperature presented in the inset. High-temperature L–I curves of (c) 4 μm × 1 mm and (d) 2 μm × 1.5 mm QW2 laser on GoPS under CW operation with the characteristic temperature shown in the inset.

To sum up, both material characterization and device performance indicate that the InGaAs/GaAs/GaAsP QW structure is better than InGaAs/GaAs QW on Si.

In conclusion, by adopting strain-compensated InGaAs/GaAs/GaAsP QWs as the gain media, we have demonstrated the CW mode operation of 980 nm QW lasers on (001) Si at RT. The lowest threshold current density obtained was 550 A/cm^2. A total power exceeding 35 mW was achieved with the QW2 laser structure, lasing up to 95 °C. A comparison of the two different QW laser structures in terms of device performance was made. The QW structure with the tensile-strained GaAsP barriers shows lower threshold current density and better temperature stability than conventional InGaAs/GaAs QW in laser devices, which is favorable for 980 nm QW lasers on Si. The realization of QW lasers directly grown on Si provides a straightforward and potential low-cost approach toward realizing III–V lasers on Si by optimizing heteroepitaxy of III–V materials on Si.

This work was supported in part by the Research Grants Council, University Grants Committee (No. 16213420), and in part by the Innovation and Technology Fund (Nos. ITS/201/19FP and ITS/226/21FP). The authors would like to thank the Material Characterization and Preparation Facility (MCPF) and Nanosystem Fabrication Facility (NFF) of HKUST for technical support and discussion. Helpful discussions with Dr. Y. Xue is acknowledged.

AUTHOR DECLARATIONS

Conflict of Interest

The authors have no conflicts to disclose.

Author Contributions

J.H. and Q.L. contributed equally to this work.

Jie Huang: Writing – original draft (lead). **Qi Lin:** Writing – review & editing (equal). **Wei Luo:** Writing – review & editing (equal). **Wen Gu:** Writing – review & editing (equal). **Liying Lin:** Writing – review & editing (equal). **Kei May Lau:** Supervision (lead); Writing – review & editing (equal).

DATA AVAILABILITY

The data that support the findings of this study are available from the corresponding author upon reasonable request.

REFERENCES

[1]D. Thomson, A. Zilkie, J. E. Bowers, T. Komljenovic, G. T. Reed, L. Vivien, D. Marris-Morini, E. Cassan, L. Virot, J. M. Fédéli, J. M. Hartmann, J. H. Schmid, D. X. Xu, F. Boeuf, P. O'Brien, G. Z. Mashanovich, and M. Nedeljkovic, J. Opt. **18**, 073003 (2016).
[2]Q. Li and K. M. Lau, Prog. Cryst. Growth Charact. Mater. **63**, 105 (2017).
[3]J. C. Norman, D. Jung, Z. Zhang, Y. Wan, S. Liu, C. Shang, R. W. Herrick, W. W. Chow, A. C. Gossard, and J. E. Bowers, IEEE J. Quantum Electron. **55**, 2000511 (2019).
[4]Z. Zhou, B. Yin, and J. Michel, Light. Sci. Appl. **4**, e358 (2015).
[5]A. W. Fang, H. Park, O. Cohen, R. Jones, M. J. Paniccia, and J. E. Bowers, Opt. Express **14**, 9203 (2006).
[6]N. Fujioka, T. Chu, and M. Ishizaka, J. Lightwave Technol. **28**, 3115 (2010).
[7]M. J. R. Heck, J. F. Bauters, M. L. Davenport, J. K. Doylend, S. Jain, G. Kurczveil, S. Srinivasan, Y. Tang, and J. E. Bowers, IEEE J. Select. Top. Quantum Electron. **19**, 6100117 (2013).
[8]Y. Zhang, Q. Du, C. Wang, T. Fakhrul, S. Liu, L. Deng, D. Huang, P. Pintus, J. Bowers, C. A. Ross, J. Hu, and L. Bi, Optica **6**, 473 (2019).
[9]B. Shi, S. Zhu, Q. Li, C. W. Tang, Y. Wan, E. L. Hu, and K. M. Lau, Appl. Phys. Lett. **110**, 121109 (2017).
[10]M. Yamaguchi, M. Tachikawa, Y. Itoh, M. Sugo, and S. Kondo, J. Appl. Phys. **68**, 4518 (1990).
[11]L. Megalini, B. C. Cabinian, H. Zhao, D. C. Oakley, J. E. Bowers, and J. Klamkin, J. Electron. Mater. **47**, 982 (2018).
[12]R. Alcotte, M. Martin, J. Moeyaert, R. Cipro, S. David, F. Bassani, F. Ducroquet, Y. Bogumilowicz, E. Sanchez, Z. Ye, X. Y. Bao, J. B. Pin, and T. Baron, APL Mater. **4**, 046101 (2016).
[13]Z. Yan, Y. Han, and K. M. Lau, J. Appl. Phys. **128**, 035302 (2020).
[14]R. Fischer, D. Neuman, H. Zabel, H. Morkoc, C. Choi, and N. Otsuka, Appl. Phys. Lett. **48**, 1223 (1986).
[15]B. Shi, Q. Li, and K. M. Lau, J. Cryst. Growth **464**, 28 (2017).
[16]W. Luo, L. Lin, J. Huang, Y. Han, and K. M. Lau, Opt. Lett. **46**, 4514 (2021).
[17]B. Shi and J. Klamkin, J. Appl. Phys. **127**, 033102 (2020).
[18]K. Li and W. Wang, J. Cryst. Growth **496–497**, 31 (2018).
[19]C. Shang, J. Selvidge, E. Hughes, J. C. Norman, A. A. Taylor, A. C. Gossard, K. Mukherjee, and J. E. Bowers, Phys. Status Solidi A **218**, 2000402 (2021).
[20]J. Huang, Q. Lin, W. Luo, L. Lin, and K. M. Lau, J. Appl. Phys. **132**, 193103 (2022).
[21]C. Shang, M. R. Begley, D. S. Gianola, and J. E. Bowers, APL Mater. **10**, 011114 (2022).
[22]L. Monge-Bartolome, B. Shi, B. Lai, G. Boissier, L. Cerutti, J.-B. Rodriguez, K. M. Lau, and E. Tournié, Opt. Express **29**, 11268 (2021).
[23]M. Yamada, M. Shimizu, T. Takeshita, M. Okayasu, M. Horiguchi, S. Uehara, and E. Sugita, IEEE Photonics Technol. Lett. **1**, 422 (1989).
[24]C. Jiang, H. Liu, J. Wang, X. Ren, Q. Wang, Z. Liu, B. Ma, K. Liu, R. Ren, Y. Zhang, S. Cai, and Y. Huang, Appl. Phys. Lett. **121**, 061102 (2022).
[25]A. Jasik, A. Wnuk, J. Gaca, M. Wójcik, A. Wójcik-Jedlińska, J. Muszalski, and W. Strupiński, J. Cryst. Growth **311**, 4423 (2009).
[26]C. Weisbuch, R. Dingle, A. C. Gossard, and W. Wiegmann, Solid State Commun. **38**, 709 (1981).
[27]S. Seki and K. Yokoyama, J. Appl. Phys. **74**, 4242 (1993).
[28]G. Zhang and A. Ovtchinnikov, Appl. Phys. Lett. **62**, 1644 (1993).
[29]Y. Xue, W. Luo, S. Zhu, L. Lin, B. Shi, and K. M. Lau, Opt. Express **28**, 18172 (2020).
[30]Q. Lin, J. Huang, L. Lin, W. Luo, W. Gu, and K. M. Lau, Opt. Express **31**, 15326 (2023).
[31]J. W. Pan and J. I. Chyi, IEEE J. Quantum Electron. **32**, 2133 (1996).
[32]W. Choi, P. D. Dapkus, and J. J. Jewell, IEEE Photonics Technol. Lett. **11**, 1572 (1999).
[33]N. Tansu, D. Zhou, and L. J. Mawst, IEEE Photonics Technol. Lett. **12**, 603 (2000).
[34]B. Zhang, H. Wang, X. Wang, Q. Wang, J. Fan, Y. Zou, and X. Ma, J. Alloys Compd. **872**, 159470 (2021).
[35]X. Chen, Y. Xiao, Y. Cheng, Z. Zhang, Y. Gou, and J. Wang, J. Alloys Compd. **922**, 166173 (2022).